CHAPTER FOUR

# WALL-TO-FLUID HEAT TRANSFER

## Flow zones definition and Turbulence model test and selection

In this chapter, a packed bed used as a heat exchanger will be considered. Fluid may be heated from the column wall while flowing through a packed bed. In such a packed bed operated under steady-state conditions, a difference in local temperature between the fluid and the particle may exist, but the overall solid and fluid temperature profiles are considered to be identical to each other, as sketched in Figure 4-1. In estimating the overall steady-state temperature profiles, the heterogeneous packed bed may be assumed to be a homogeneous single phase. The temperature profiles in the bed are then predicted in terms of effective thermal conductivities and wall heat transfer coefficients.

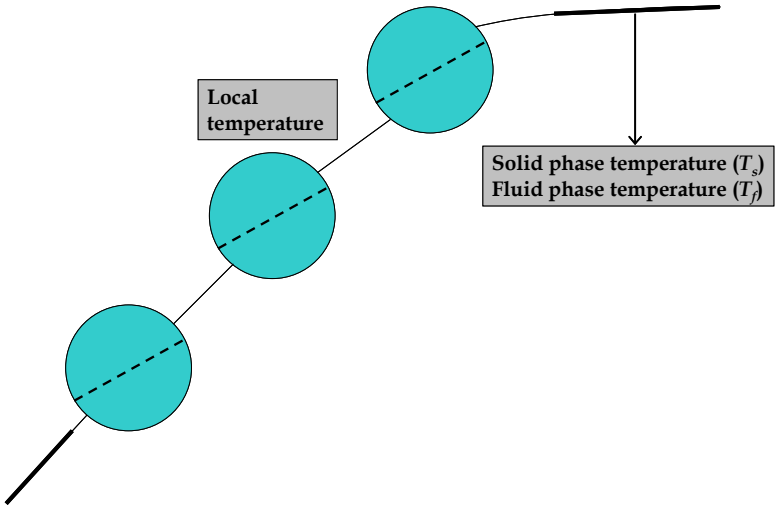


**Figure 4-1.** Steady-state temperature profiles in a packed bed (of heat exchanger type)

In the following sections, analytical solutions of the steady-state temperature profiles will be shown. In addition, a **CFD** simulation strategy for the estimation of effective thermal conductivities as well as wall heat transfer coefficients is discussed. Estimated heat transfer parameters will be compared to broadly accepted correlations, and also the simulation data will be used to analyze the numerical response of the different flow regimes and the performance of turbulence models in the prediction of *wall-to-fluid* heat transfer in packed beds.

## 4.1. GEOMETRICAL MODEL

Geometrical modeling is one of the most critical stages in **CFD** simulation; correct definition of the geometry provides a more realistic scenario for the simulation, and the technique used for constructing the geometry will ensure the feasibility of generating a mesh good enough to capture all of the phenomena involved in the problem.

The first step was to select a proper arrangement for the packed bed. In a bed with a mixture of particle sizes if average particle size is used in the calculations, heat and mass dispersion follow the predictions for a bed of monosized particles (Guedes de Carvalho and Delgado, 2000). Therefore, a homogeneous sphere stack was selected for this study. Regular packing (i.e., a simple cubic or hexagonal lattice) does not offer good *wall-to-particle* contact unless the tube-to-particle diameter ratio is 2. Other diameter ratios lead to large empty spaces near the wall, which generate high-speed flow channels at the wall and, therefore, a bad flow distribution and incorrect calculation of parameters. Preliminary tests on the aforementioned were done using a finite element **CFD** code (Guardo et al., 2003). A maximum space-occupying arrangement must

be used to simulate a more realistic case. So, a 2D approach to the circle packing theory is used to build a unit-cell and then extrapolate it to 3D geometry.

Circle packing is an arrangement of circles inside a given boundary such that no two of them overlap and some (or all) of them are mutually tangent. Solutions for the smallest diameter circles into which $n$ unit circles can be packed have been proved optimal for $1 \leq n \leq 65$ (Graham et al., 1998). Furthermore, for certain values of $n$, several distinct optimal configurations are possible. In this case, following the instructions of Melissen (1994) for building the 2D model, an 11-circle arrangement with a diameter ratio equal to 3.923+ was chosen for the 3D extrapolation.

Figure 4.2 shows the 2D model mentioned above. An 11-sphere arrangement, with 9 particle-to-wall contact points and 14 particle-to-particle contact points, was built on the basis of the preceding 2D approach. A four-layer arrangement (44 spheres) with a 60° rotation around the reactor axis within each layer was chosen as the geometrical model for **CFD** simulations. Figure 4.3 shows a lateral and isometric view of the constructed geometry, respectively.

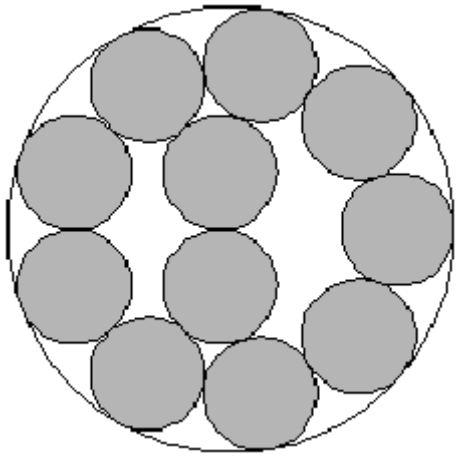

**Figure 4.2.** 2D model obtained from a transversal cut through a unit cell

The construction of *wall-to-particle* and *particle-to-particle* contact points is also an important subject in model generation. Previous work reports no contact points between surfaces (Dalman et al., 1986; Lloyd and Boehm, 1994), or the emulation of contact points (leaving small gaps between surfaces and assuming zero velocity in the gap) to avoid convergence problems (Logtenberg et al., 1999; Dixon and Nijemeisland, 2001; Guardo et al., 2003). In this study, to include real contact points, the spheres were modeled overlapping by 1% of their diameters with the adjacent surfaces in the geometric model. Convergence problems were not detected during simulation runs.

The modeled geometry was constructed following the bottom-up technique (generating surfaces and volumes from nodes and edges) to control the mesh size around critical points (i.e., *particle-to-particle* and *particle-to-wall* contact points). This was necessary to avoid grid element skewness and also to gain computational resources by reducing the number of elements in zones of low interest (i.e., geometrical zones away from contact points or away from the walls).

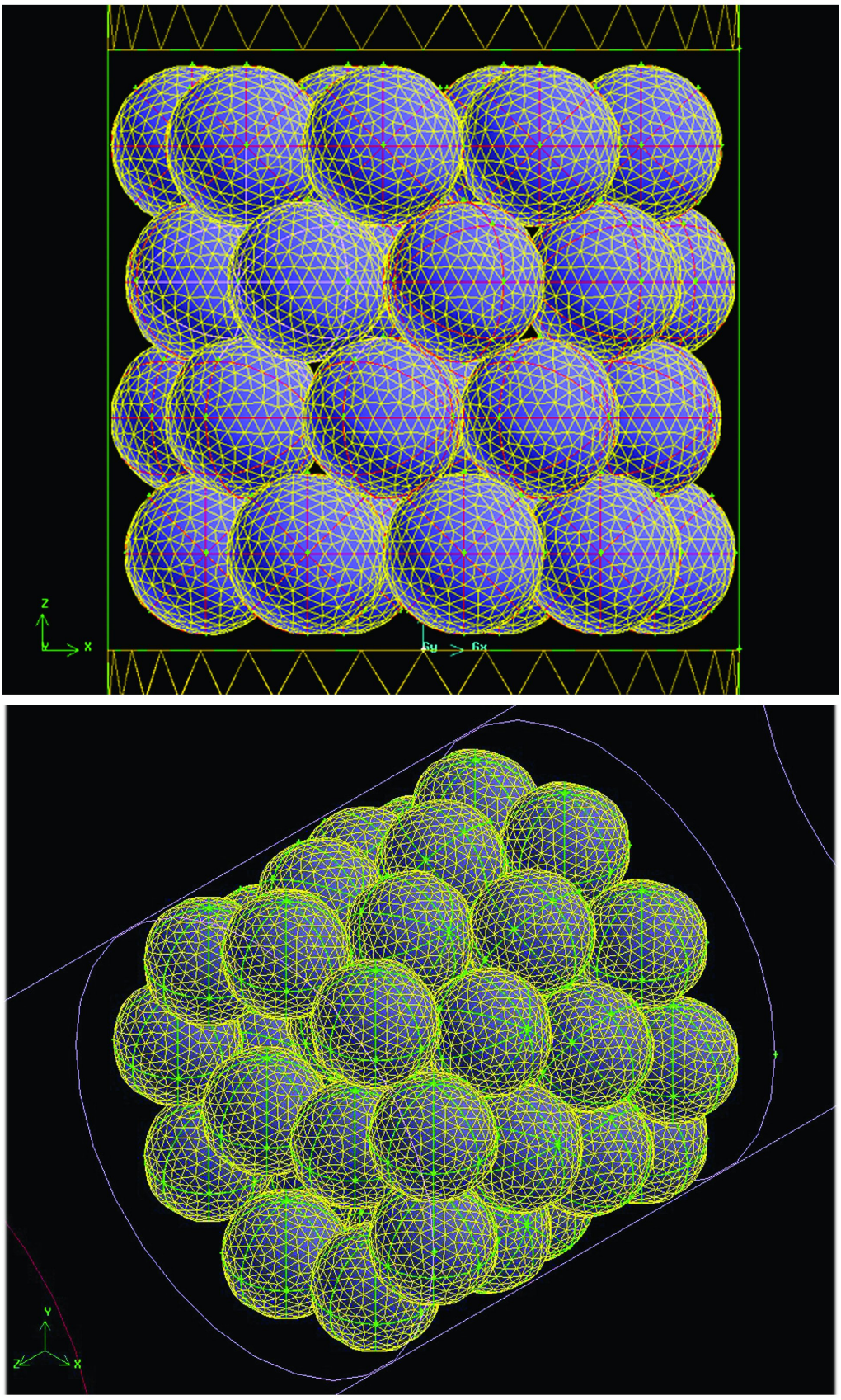


**Figure 4.3.** Lateral and isometric view of the generated geometrical model

## 4.2. MESH DESIGN AND CFD MODELING

To properly design a mesh capable of capturing the transport mechanisms present in the study in detail, a dimensionless analysis of Navier-Stokes equations under simulation conditions was developed. The dimensionless equations corresponding to mass, momentum, and energy balances are detailed in Chapter two. The orders of magnitude of the dimensionless groups were estimated by taking physical-chemical property values for air from experimental data and empirical correlations available in the literature (Reid et al., 1987; Yaws, 1999; Poling et al., 2000). Reynolds number was calculated using particle diameter as characteristic length. Reynolds analogy was used to estimate values of $Pr_t$ from $Re_t$ (White, 1991). For first analysis purposes, $Pr_t$ was assumed as a constant value within the bed, justified in the fact that majority of experimental results shows a range of variations between $0.75 < Pr_t < 2$ for air and water (Kays, 1994). Boundary (operating) conditions for each analyzed situation are shown in Table 4.1. Details on the dimensionless numbers used can be found in Appendix C. Results of the order of magnitude of the dimensionless groups are shown in Table 4.2.

| Boundary condition | Value |
|---|---|
| Circulating fluid | Air |
| Packing material | Aluminum |
| Fluid temperature at the inlet, K | 298 |
| Wall temperature, K | 423 |
| Pressure, Pa | 101325 |
| Fluid velocity at the inlet, m/s | $7.5 \times 10^{-2}$ – $7.5 \times 10^{-1}$ |
| Flow models | Laminar<br>Spalart – Allmaras<br>$\kappa - \varepsilon$ family<br>$\kappa - \omega$ |

**Table 4.1.** Boundary (operating) conditions for analyzed cases

| | | | |
|---|---|---|---|
| ***Re*** | $10^{1}$ | $10^{2}$ | $10^{3}$ |
| ***Sr*** | $10^{1}$ | $10^{0}$ | $10^{-1}$ |
| ***Ma*** | $10^{-5}$ | $10^{-4}$ | $10^{-3}$ |
| ***Eu*** | $10^{1}$ - $10^{3}$ | $10^{-1}$ - $10^{1}$ | $10^{-1}$ |
| ***Fr*** | $10^{-4}$ - $10^{-2}$ | $10^{-2}$ - $10^{0}$ | $10^{0}$ |
| ***Pr*** | $10^{-1}$ | $10^{-1}$ | $10^{-1}$ |
| ***Ec*** | $10^{-10}$ - $10^{-8}$ | $10^{-8}$ - $10^{-6}$ | $10^{-6}$ |
| $Re_t$ | $10^{0}$ | $10^{0}$ | $10^{0}$ |
| $Pr_t$ | $10^{-1}$ | $10^{-1}$ | $10^{-1}$ |

**Table 4.2.** Dimensionless groups' magnitude orders

In the cases analyzed of *wall-to-fluid* heat transfer at low pressure, dimensionless analysis allows us to identify the problem as forced convection heat transfer in laminar, transition or turbulent flow regimes. For the momentum balance (Equation 2.1-26) it becomes clear that viscous forces decrease their contribution as ***Re*** increases. Inertial gravity forces increase their contribution as ***Re*** decreases, and pressure drop together with turbulent forces become the most important terms in the momentum balance at high ***Re***. In the energy balance (Equation 2.1-28), the convective and the diffusive term become the most important terms. For both balances, steady-state analysis can be used.

Accurate modeling of the flow mixing in this case implies using a highly refined homogeneous mesh, but this requires many computational resources. One of the aims of this part of the work was to verify whether accurate modeling is possible if the homogeneous mesh requirement is relaxed, to minimize simulation times. Theoretically, the mesh should be able to appropriately define the boundary layer around the geometry present in the model for the laminar solution. In the case of a turbulent solution, mesh density will depend on the *near-wall* modeling strategy adopted for resolving the problem and will be determined by the characteristic $y^+$ parameter (Coussirat, 2003). According to this, the mesh should be designed to properly define a minimum cell size to capture in a suitable way the computed variables on the proposed geometry. Therefore, a mesh sensitivity analysis should be done for those models applying wall functions (such as the $\kappa - \varepsilon$ family models).

Transition from laminar to turbulent flow in packed beds has not been extensively studied with numerical **CFD** simulation, and there are still doubts about when the turbulent model should be activated, because there are no reliable guidelines to predict the flow transition in complex geometries, such as packed bed reactors or extraction equipment. Experimental studies have found that a transition from laminar to turbulent flow in a damped bed of spheres occurs over the range from 110 to 150 for the Reynolds number, and that around $Re \approx 300$ the flow pattern is turbulent (Jolls and Hanratty, 1952). Other authors have stated that a transition from laminar to turbulent flow occurs at $Re \approx 100$ (Tobis and Ziólkowski, 1988). These results should be used as an indicator of when it is necessary to activate a turbulent model. Preliminary work done with a finite element **CFD** code showed that laminar to turbulent flow transition could be estimated between $110 < Re < 150$ (Guardo et al., 2002). In this section, laminar and turbulent flow solutions are calculated using a finite volume **CFD** code, and shown to compare their performances. For the turbulent solutions, the turbulence intensity boundary condition at the bed inlet was set to 4%, as estimated from common pipe flow equations. To verify the choice of the turbulence intensity parameter, a simulation was run applying a lower value of this parameter, with no significant change in the results obtained. Although physically the variation of the turbulence intensity at the flow inlet can generate changes in flow behavior, numerically these changes are not detected by most of the turbulence models when the difference between the imposed value and the real value is reasonable (Coussirat, 2003).

## 4.3. MODEL SETUP

Navier – Stokes equations and energy balance were solved using commercially available finite volume code software Fluent 5.0 (Fluent Inc., 1998). The fluid was taken to be incompressible, Newtonian, and in a laminar or turbulent flow regime due to the impossibility of **RANS** models to capture flow transition. Air was chosen as the simulation fluid, for which the constants were available in the software database. The incompressible ideal gas law (for density) and the power law (for viscosity) were applied to the model to make these variables temperature-dependent.

Simulations were run on an HP C3000 workstation, and simulation times ranged from 12 to 48 hours depending on the case studied. Second-order upwind discretization schemes were

selected to compute the field variables. The pressure-velocity coupling algorithm was the SIMPLE scheme. This scheme derives an equation for the pressure from the discrete continuity equation (Fluent Inc., 1998). Numerical convergence of the model was checked on the basis of the residuals of all computed variables. For more complete convergence verification, the drag force over particle surfaces and the average static temperature at the bed outlet were also chosen as monitors.

## 4.4. RESULTS AND DISCUSSION

The objective of this part of work was to test **CFD** response to different flow regimes and to test the capabilities of **CFD**-implemented **RANS** models applied to packed bed reactor design. Simulations were run for several values of ***Re*** (see Table 4.3) with constant temperatures at the bed inlet and wall. Slight differences in the values of ***Re***, $\rho$, and $\mu$ could be observed among laminar and turbulent simulations with an identical inlet velocity.

| Velocity (m/s) | Laminar | Spalart – Allmaras | $\kappa-\omega$ | $\kappa-\varepsilon$ | | |
|---|---|---|---|---|---|---|
| | | | | Standard | RNG | Realizable |
| | | | *Re* | | | |
| 0.0750 | 85 | | | | | |
| 0.1125 | 133 | 130 | 131 | 127 | 131 | 128 |
| 0.1500 | 177 | 175 | 175 | 170 | 172 | 171 |
| 0.2250 | 265 | 265 | 260 | 259 | 261 | 260 |
| 0.3750 | 447 | 448 | 439 | 438 | 441 | 440 |
| 0.5250 | | 633 | 621 | 619 | 622 | 621 |
| 0.7500 | | 912 | 894 | 893 | 897 | 894 |

**Table 4.3.** Velocity conditions applied to **CFD** model and obtained ***Re*** for each case

The real packed bed flow problem was approached by means of nonregular packing modeling. Standard correlations for pressure drop and heat transfer parameters were selected as reference values to be compared against the numerical results generated. The use of "real" contact points was successfully included during model generation. The **CFD** model was solved for both laminar and turbulent flow situations, and buoyancy terms were activated for low ***Re*** simulations. For turbulence modeling, the Spalart-Allmaras, standard, **RNG** and realizable $\kappa-\varepsilon$, and the $\kappa-\omega$ turbulence models were used and their results compared. Details of turbulence models can be found in Appendix B. The results of the simulations are discussed below.

### 4.4.1. VELOCITY PROFILES

To study the velocity distribution along the packed bed, axial and radial cuts were made along the packed bed to generate velocity vector plots. Velocity profiles were also observed in the *near-wall* region of the modeled arrangements.

As expected, in all of the cases analyzed, flow channeling took place near the wall and inside the bed, due to the presence of constrained flow areas. Strong radial flow from the middle to the wall was also noticeable. Due to the channeling of the flow (strong axial flow and reduced radial flow) at the wall, the local radial heat transfer rate decreases, causing the well-known

"temperature jump" near the wall. Figures 4.4 and 4.5 illustrate the *near-wall* flow and the velocity profiles along a transversal cut in the packed bed.

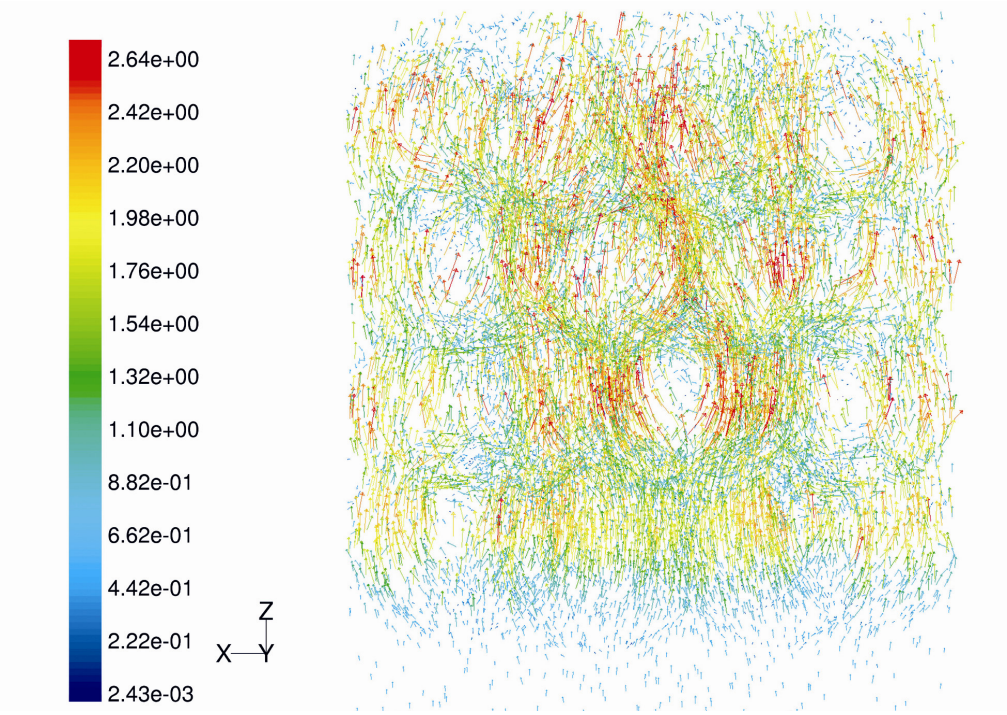


**Figure 4.4.** Velocity vectors profile near the wall for ***Re*** = 633
Velocity profile is expressed in m/s

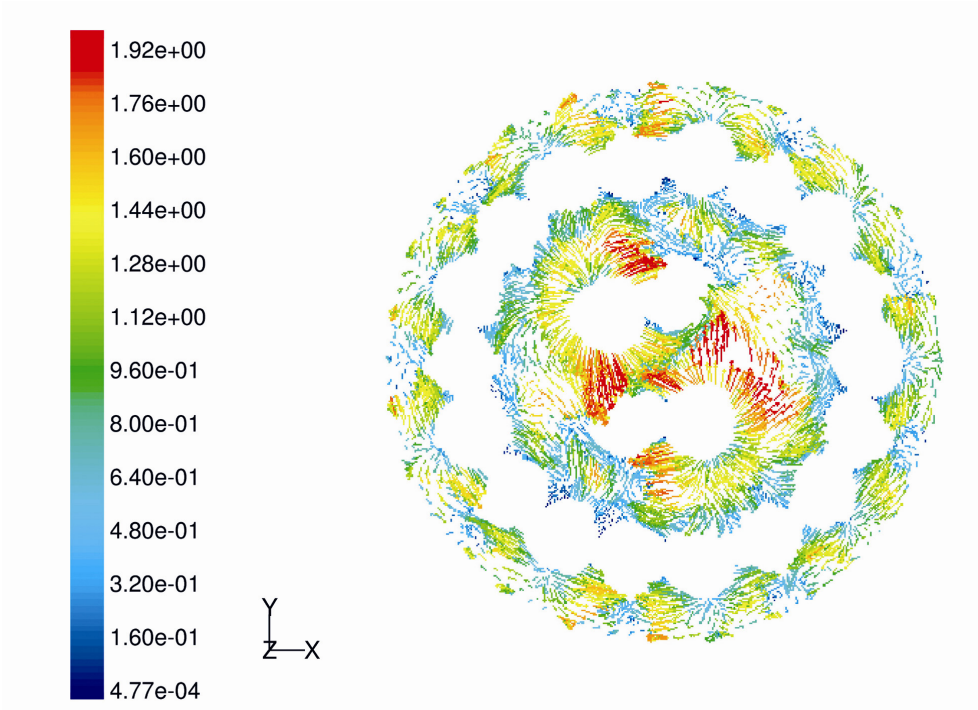


**Figure 4.5.** Velocity vectors profile along a transversal cut ($z = 0.0375\ m$) for ***Re*** = 448
Velocity profile is expressed in m/s

It was also noticed that velocity increased by up to 4 times the inlet velocity in some constrained areas of the packed bed. Stagnation points and secondary flows were noticed near the contact points (see Figure 4.6). As ***Re*** increases, within the range of velocities studied, eddy flow becomes easier to identify around the spheres, for both simulated turbulence models. All of the features mentioned above are also found by Suekane et al., (2003) who used a magnetic resonance imaging technique to directly measure the velocity of flow in a pore space that models a simply packed bed.

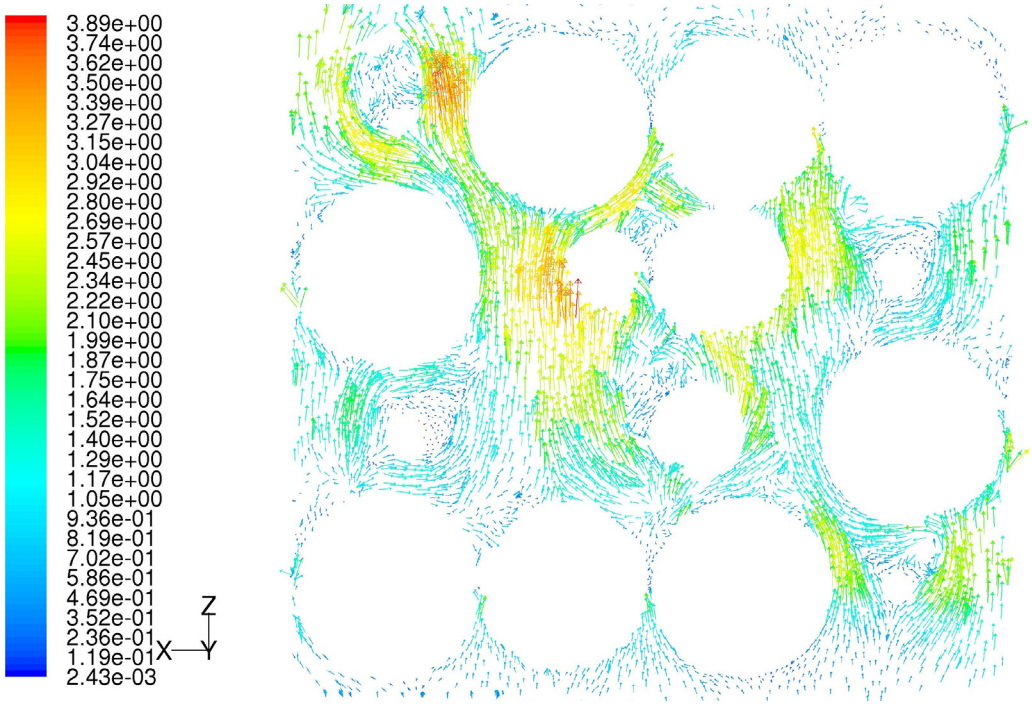


**Figure 4.6.** Velocity vectors profile in a cross section ($y = 0$) for ***Re*** = 633
Velocity profile is expressed in m/s

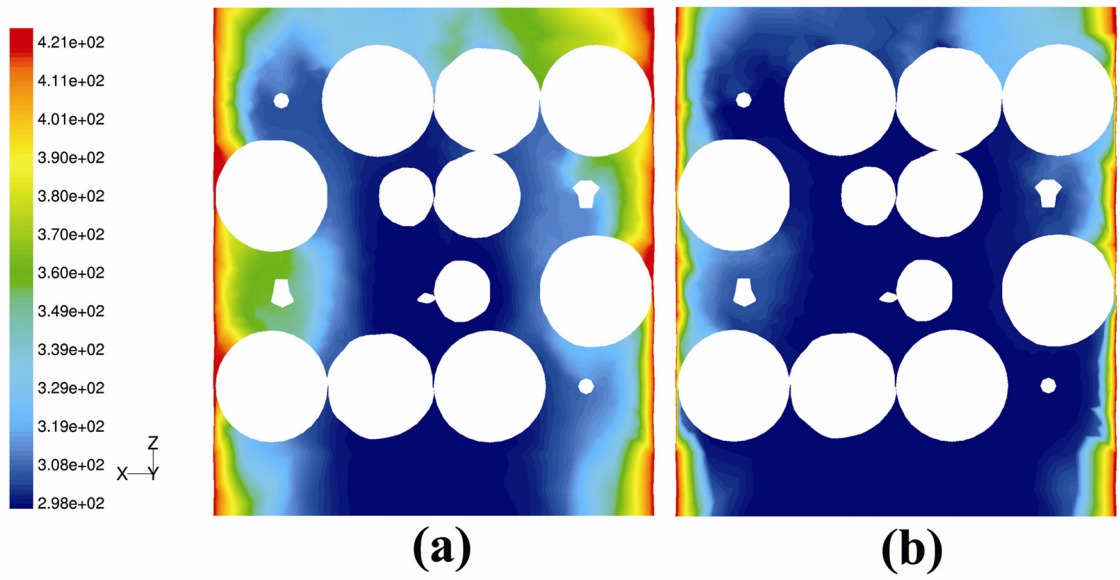


**Figure 4.7.** Temperature contours in a cross section ($y = 0$) for *(a)* ***Re*** = 84 and *(b)* ***Re*** = 893 applying standard $\kappa - \varepsilon$ turbulence model
Temperature profile expressed in K

## 4.4.2. TEMPERATURE CONTOURS

Figure 4.7 shows temperature contour plots for two different model simulations (***Re*** = 84 and ***Re*** = 893) to illustrate how the temperature field changed with flow rate. It shows a strong influence of the fluid flow pattern on temperature profiles. The temperature profiles penetrate the bed faster for low ***Re*** than for high ***Re*** flow patterns, because the mixing in the zones nearest the wall increases as ***Re*** increases.

Analyzing the kinetic energy ($\kappa$) profiles obtained with the $\kappa-\varepsilon$ model simulations, the aforementioned idea becomes clear (see Figure 4.8). A comparison between the two selected cases shows increasing kinetic energy inside the packed bed with increasing ***Re***. The temperature profiles show that the idea of thinking of one single value of Nuw for the whole packed bed is not realistic; however, it can be useful for equipment design.

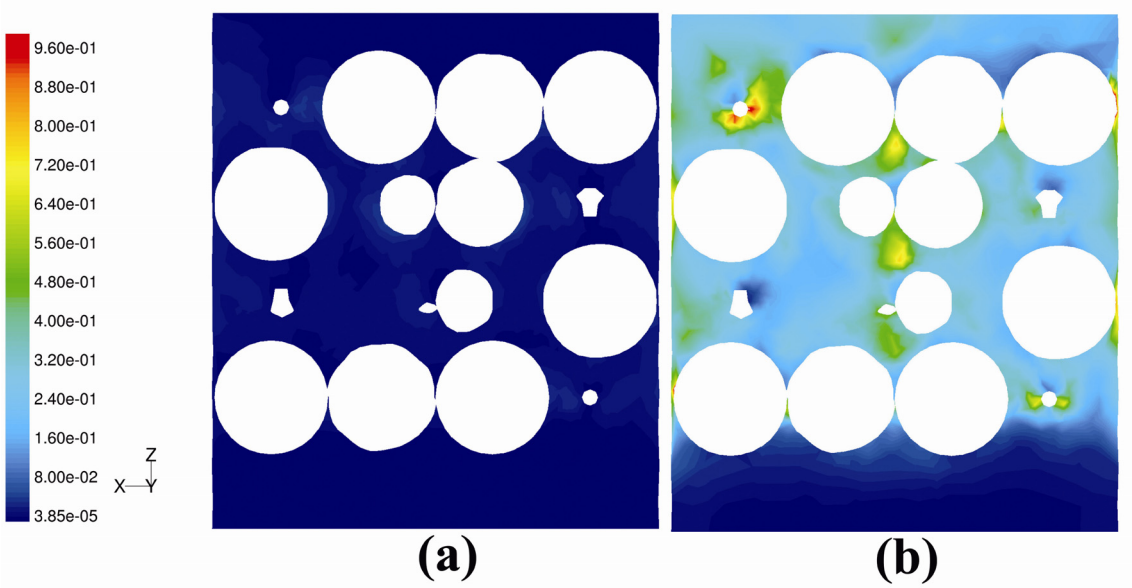


**Figure 4.8.** Kinetic energy contours in a cross section ($y$ = *0*) for *(a)* ***Re*** = 84 and *(b)* ***Re*** = 893 applying standard $\kappa-\varepsilon$ turbulence model
Kinetic energy profile expressed in $m^2/s^2$

## 4.4.3. PRESSURE DROP ALONG THE BED

The results obtained using **CFD** simulation for the pressure drop along the bed were compared to Ergun's correlation (1952) for pressure drop in beds packed with spherical particles. Average density and viscosity of the fluid within the bed were taken for Ergun's equation calculations. See Figure 4.9 for details.

All of the models used (laminar, Spalart – Allmaras, $\kappa-\omega$ and $\kappa-\varepsilon$ family models) show good agreement with Ergun's equation. This can be explained by the fact that the velocity fields obtained for laminar and turbulent solutions are similar. The pressure drop calculation is intrinsically related to the velocity field and is not affected by mixing parameters or additional diffusive terms included within the different models' equations.

In the case of turbulence modeling, the results from the Spalart - Allmaras model show a slightly better agreement with Ergun's prediction of the frictional pressure drop in the packed bed than those from the standard $\kappa-\varepsilon$ model. The better *near-wall* treatment in the Spalart -

Allmaras model under the meshing conditions used for simulations favors velocity-pressure coupling and the estimation of drag coefficients over the involved surfaces. The situation is similar when estimating heat transfer parameters. A more complete discussion of the influence of the *near-wall* treatment on parameter estimates can be found in the following sections.

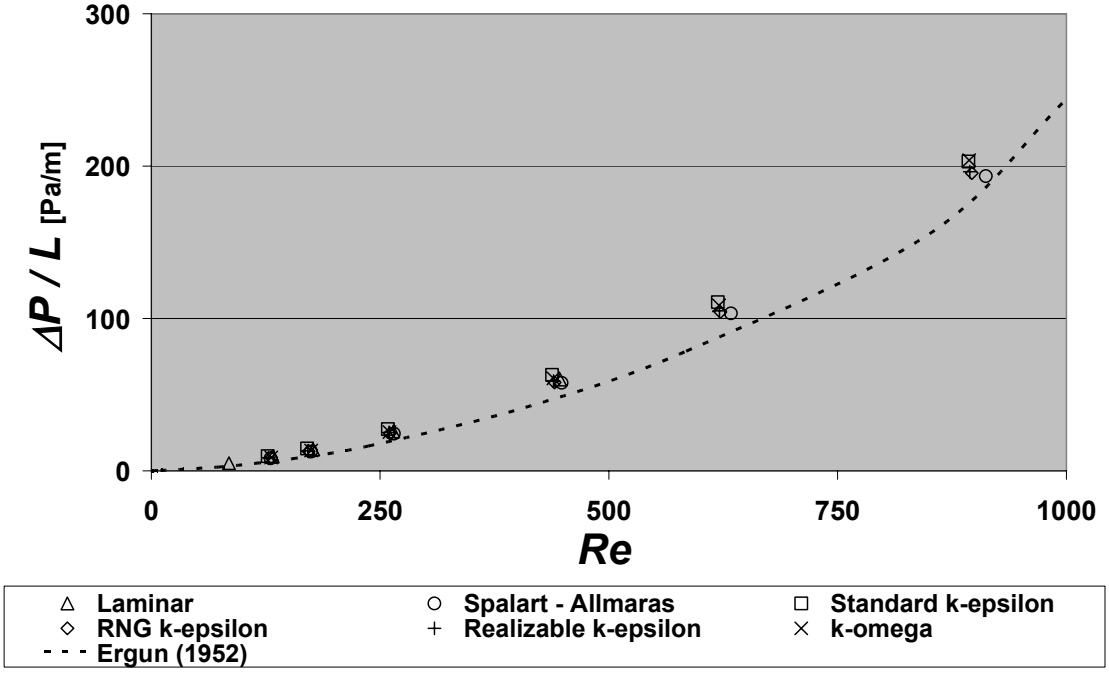


**Figure 4.9.** Pressure drop along the bed vs. ***Re***

## 4.4.4. Determination of effective radial thermal conductivities and wall heat transfer coefficients

For a cylindrical packed bed operated as a steady-state heat exchanger, the heat balance equation gives

$$GC_{p,f}\frac{\partial T}{\partial z} = k_r \frac{1}{r}\frac{\partial}{\partial r}\left(r\frac{\partial T}{\partial r}\right) + k_{ax}\left(\frac{\partial^2 T}{\partial x^2}\right) \qquad [4.4\text{-}1]$$

At intermediate and high flow rates, the axial second derivative is very small compared to the other terms. Equation [4.4-1] then reduces to

$$GC_{p,f}\frac{\partial T}{\partial z} = k_r \frac{1}{r}\frac{\partial}{\partial r}\left(r\frac{\partial T}{\partial r}\right) \qquad [4.4\text{-}2]$$

Equation [4.4-2] was first solved by Hatta and Maeda (1948), and a few years later, by Coberly and Marshall (1951), both based on the following boundary conditions:

$$\begin{aligned} T &= T_0 && z = 0 \\ \frac{\partial T}{\partial r} &= 0 && r = 0 \\ k_r \frac{\partial T}{\partial r} &= h_w\left(T_w - T\right) && r = R \end{aligned} \qquad [4.4\text{-}3]$$

The solution to Equation [4.4-2] whit the conditions given by Equation [4.4-3] is:

$$\frac{T_w - T}{T_w - T_0} = 2\sum_{n=1}^{\infty} \frac{J_0\left(a_n r/R\right) e^{-a_n^2 y}}{a_n\left(1 + \left(a_n/Bi\right)^2\right) J_1\left(a_n\right)} \qquad [4.4\text{-}4]$$

where

$$y = \frac{k_r z}{G C_{p,f} R^2} \qquad [4.4\text{-}5]$$

***Bi*** is the Biot number (see Appendix C for details) and $a_n$ is an *n-th* root of the following equation of Bessel functions ($J_0$ is a Bessel function of first kind and zeroth-order and $J_1$ is that of first kind and first-order):

$$Bi J_0\left(a_n\right) = a_n J_1\left(a_n\right) \qquad [4.4\text{-}6]$$

When ***y***, as defined by Equation [4.4-5], is greater than about 0.2, the series in Equation [4.4-4] converges so rapidly such that only the first term of the series is significant. Therefore,

$$\frac{T_w - T}{T_w - T_0} = \frac{2 J_0\left(a_1 r/R\right) e^{-a_1^2 y}}{a_1\left(1 + \left(a_n/Bi\right)^2\right) J_1\left(a_1\right)} \qquad [4.4\text{-}7]$$

where

$$Bi J_0\left(a_1\right) = a_1 J_1\left(a_1\right) \qquad [4.4\text{-}8]$$

Equation [4.4-7] gives the temperature profile deep in the bed. At $r = 0$ $(T = T_c)$, Equation [4.4-7] reduces to

$$\frac{T_w - T_c}{T_w - T_0} = \frac{2 e^{-a_1^2 y}}{a_1\left(1 + \left(a_n/Bi\right)^2\right) J_1\left(a_1\right)} \qquad [4.4\text{-}9]$$

which gives the temperature profile along the central axis of the bed under the conditions specified.

The two heat transfer parameters, $k_r$ and $h_w$, are easily determined from measurements of axial temperature profiles. The temperature profiles at any radial position will do, but the temperature measurements along the central axis of the bed, where radial temperatures level off, are most preferable.

If the measured temperatures at the center of the bed, $T_c$, are plotted as $ln\,[(T_w - T_c)/(T_w - T_0)]$ versus $z$, a straight line will be produced at sufficiently large values of $z$. This straight line means that this is the region where Equation [4.4-9] holds. Figure 4.10 shows an example of the aforementioned for a simulation case.

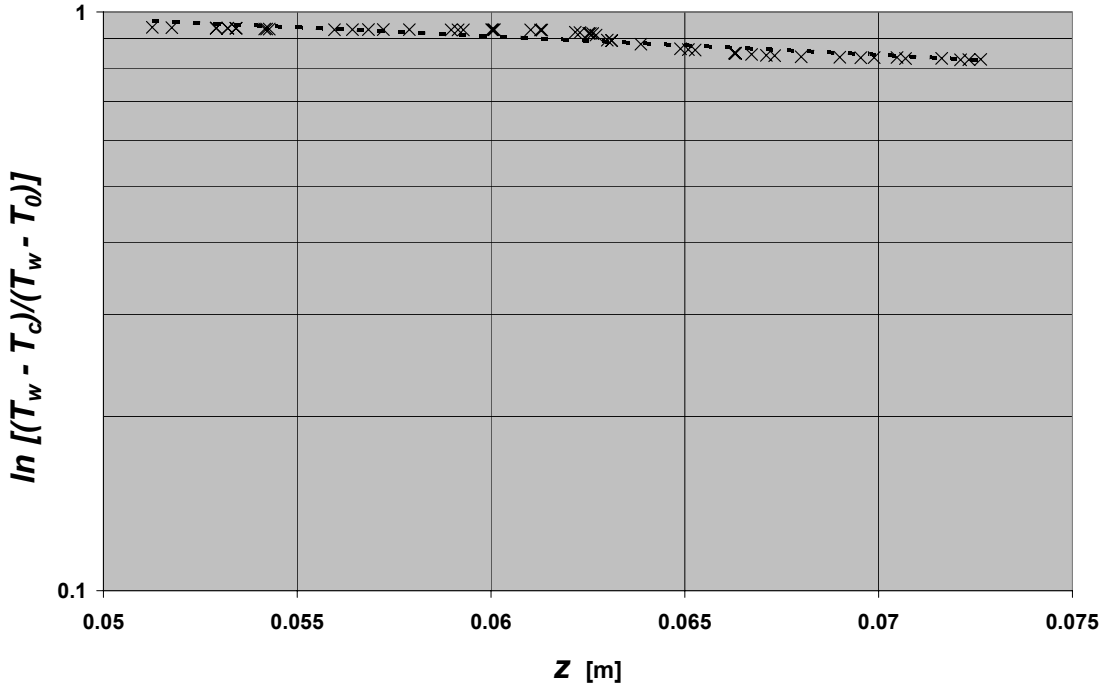


**Figure 4.10.** **CFD** obtained temperatures vs. bed height for ***Re*** = 127 applying the standard $\kappa - \varepsilon$ turbulence model

The slope and the intercept of the straight line are

$$\textit{Slope} = -a_1^2\left(\frac{k_r}{GC_{p,f}R^2}\right) \qquad [4.4\text{-}10]$$

and

$$\textit{Intercept} = \ln\frac{2}{a_1\left(1+\left(a_1/Bi\right)^2\right)J_1\left(a_1\right)} \qquad [4.4\text{-}11]$$

Also, Equation [4.4-9] shows that, when $z$ is large, the mixed mean temperature of the effluent fluid, $T_m$, is related to $T_c$ by:

$$\frac{T_w - T_m}{T_w - T_0} = \frac{2J_1\left(a_1\right)}{a_1} \qquad [4.4\text{-}12]$$

Therefore, the parameters, $k_r$ and $h_w$, can be determined by either ***(a)*** Equations [4.4-10] and [4.4-12], or ***(b)*** Equations [4.4-10] and [4.4-11], both in conjunction with Equation [4.4-8]. In method ***(b)***, the value of $a_1$, based on Equations [4.4-10] and [4.4-11], is easily affected by a slight change in the value of the intercept obtained from the extrapolation of the linear relationship between $ln\,[(T_w - T_c)/(T_w - T_0)]$ and $z$. On the other hand, $a_1$ is more safely determined from

equation [4.4-12]. Therefore, $k_r$ and $h_w$ may, in general, be more accurately evaluated from method ***(a)*** than method ***(b).***

## 4.4.5. NUMERICAL RESPONSE TO FLOW REGIMES

To calculate the values of $Nu_w$, $k_r$, and $Bi$, $k_f$ was taken as a constant reference value ($k_f$ = 0.0242 W/m · K). The mass flow rate given by the software and the average values for the viscosity along the bed were used to calculate $Re$.

Figures 4.11 and 4.12 show the values of $Nu_w$ and $k_r/k_f$, respectively, for different $Re$ values, which was calculated according to the method explained in a previous section of this chapter. To show the influence of the flow regime on the numerical response of the **CFD** software, and therefore, on the values of $Nu_w$ and $k_r/k_f$, values for the laminar and both the Spalart-Allmaras and the standard $\kappa - \varepsilon$ turbulent solutions are shown for $Re$ between 84 and 912. The **CFD** results in Figure 4.11 for the Spalart-Allmaras and standard $\kappa - \varepsilon$ turbulent solutions show good agreement with empirical models such as those proposed by Olbrich and Potter (1972) or Dixon and Cresswell (1979) for the $Nu_w$ estimate, as opposed to the simple model proposed by Li and Finlayson (1977). These complex models take into account important factors such as pressure drop or the geometrical characteristics of the bed that are also included within the calculations of the **CFD** code for modeling the heat transfer phenomena.

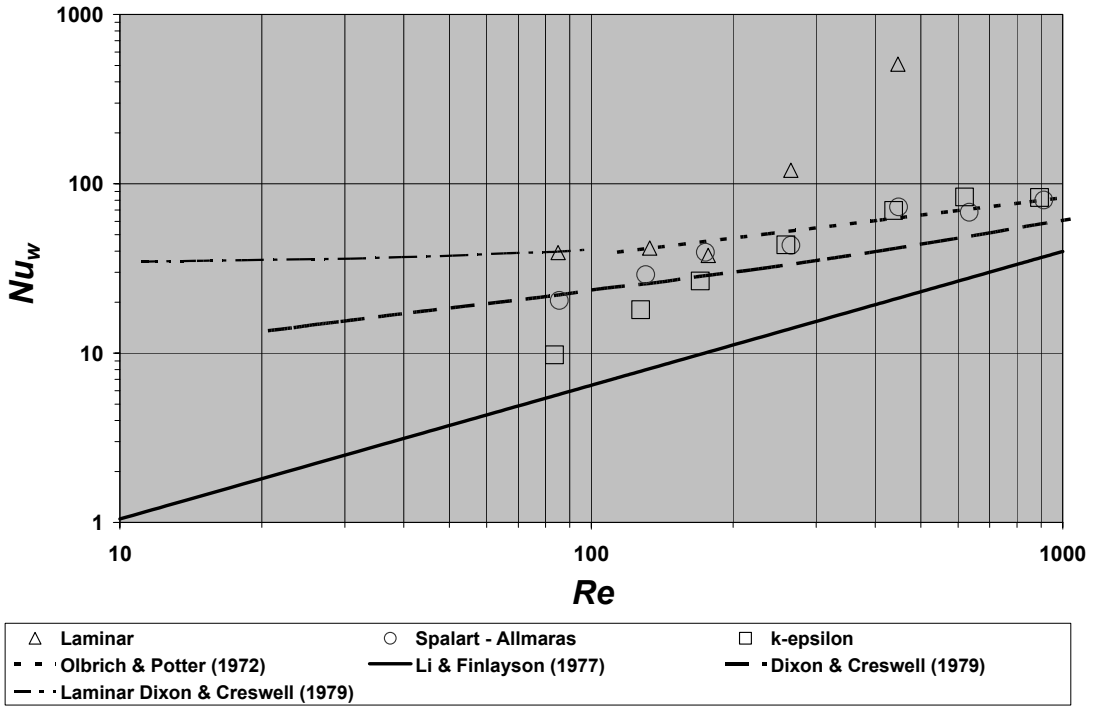


**Figure 4.11.** Nusselt number vs. Reynolds number for laminar, transition and turbulent flow regime

It is important to notice that in the transition zone, as $Re$ decreases the values obtained for $Nu_w$ tend to be underestimated if compared to the values obtained with the empirical correlations shown in the case of a turbulent solution. In the case of the laminar solution, it should be noticed that the first three values of the series ($Re$ < 177) agree excellently with the values predicted by Dixon and Creswell (1979) for laminar flow. When $Re$ = 265 and greater, the

laminar solution overestimates the value of $Nu_w$. The behavior of the solutions for the laminar and turbulent cases is in total concordance with the expected behavior of the transition from laminar to turbulent flow in a packed bed. In the transition flow regime (approximately 110 < $Re$ < 300 for fluid flow through a packed bed; Jolls and Hanratty, 1966), turbulent results must be carefully studied due to the inability of **RANS** models to predict the transition from laminar to turbulent flow (Durbin and Petterson Reif, 2001).

Estimates of effective radial conductivity ($k_r/k_f$) values from the **CFD** numerical results also agree well with accepted correlations, such as those proposed by Yagi and Wakao (1959) or Yagi and Kunii (1960) Figure 4.12 shows the obtained numerical results. Effective radial conductivity is strongly influenced by the flow velocity profile. Other factors, like the geometrical characteristics of the bed or wall coupling functions, may influence the radial conductivity estimates, but in this case their influence is not as strong as in the estimation of $Nu_w$.

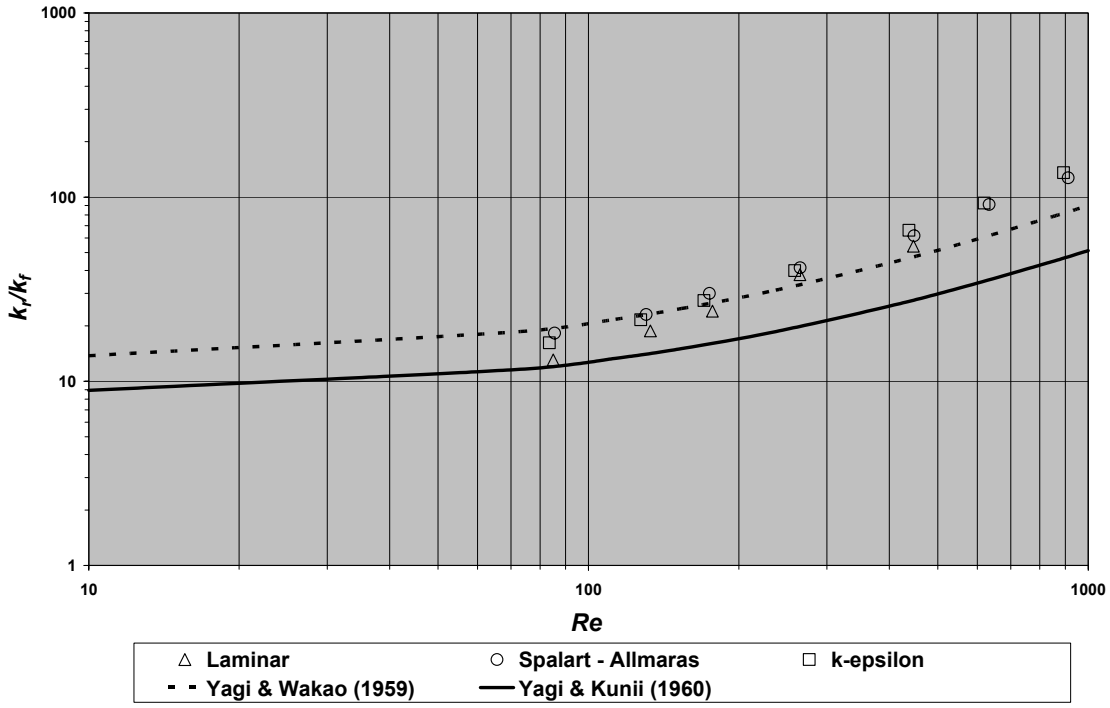


**Figure 4.12.** Radial conductivity vs. Reynolds number for laminar, transition and turbulent flow regime

**CFD** results obtained using the Spalart-Allmaras model seem to agree with the empirical correlations better than the results obtained with the $\kappa - \varepsilon$ model for the turbulent solution. A deeper study on the performance of **RANS** models in the prediction of *wall-to-fluid* heat transfer parameters is presented in the upcoming section.

## 4.4.6. TURBULENCE MODEL EVALUATION

It is of paramount importance to know the most adequate turbulence model to compute mean and local values of heat transfer coefficients in the design of packed bed reactors. The system of equations is defined by averaged continuity, momentum and energy equations. Fluctuations of these mean quantities are calculated by means of a turbulence model. In this way, representative velocity and thermal fields are obtained. Because most of the industrial interest is

to determine the mean quantities, this technique is broadly used in modeling turbulent industrial flows. The research on this subject has led to the development of several classes of turbulence models. The classification scheme shown in Appendix B was made taking only into account the models used in this work, based on the eddy viscosity concept.

The standard formulation of these models is only valid for turbulent flows far from walls where terms corresponding to shear stress are small and the turbulent viscosity becomes isotropic. Walls are the main source of vorticity and turbulence because in these regions exist large gradients of variables and the momentum transport is more vigorous. To take into account the non-isotropic nature of turbulence in *near-wall* regions, models have been refined in several forms. The "wall functions", damping functions or two-layer modeling are some examples of these refinement techniques.

To test the capabilities of **CFD**-implemented **RANS** models applied to the estimation of heat transfer parameters in packed bed reactors, standard correlations for pressure drop (see section 4.4.3) and heat transfer parameters (see section 4.4.5) were selected as reference values to compare against the numerical results generated. Simulations were run under several values of ***Re*** (see Table 4.3) and at constant temperature values at the bed inlet and at the wall (see Table 4.1 for details on the boundary conditions).

In order to calculate the values of $Nu_w$, $k_r$, and ***Bi***, $k_f$ was taken as a constant reference value ($k_f$ = 0.0242 W/m · K). Computed values of $Nu_w$ and $k_r/k_f$ at several ***Re*** are shown, in Figures 4.13 and 4.14, respectively. These values were calculated according to calculation methods previously explained (see section 4.4.4). Values for the different turbulence model solutions are shown for $127 < Re < 912$, to show the influence of the choice of the turbulence model on the heat transfer parameters.

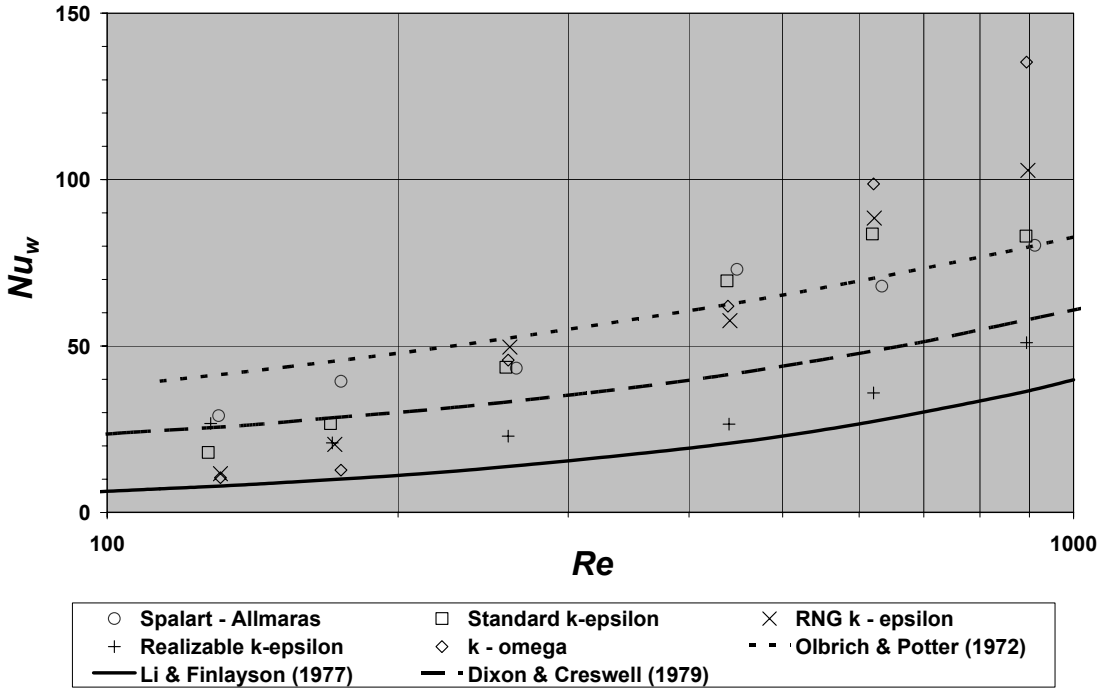


**Figure 4.13.** Nusselt number vs. Reynolds number for different **RANS** models

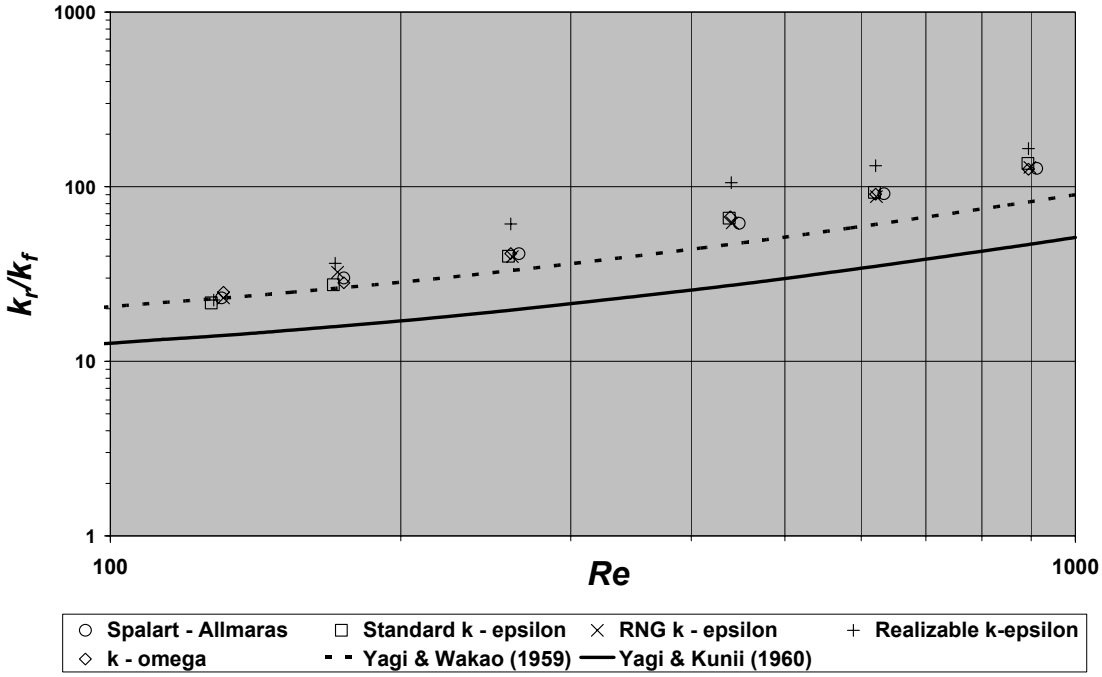


**Figure 4.14.** Thermal conductivity vs. Reynolds number for different **RANS** models

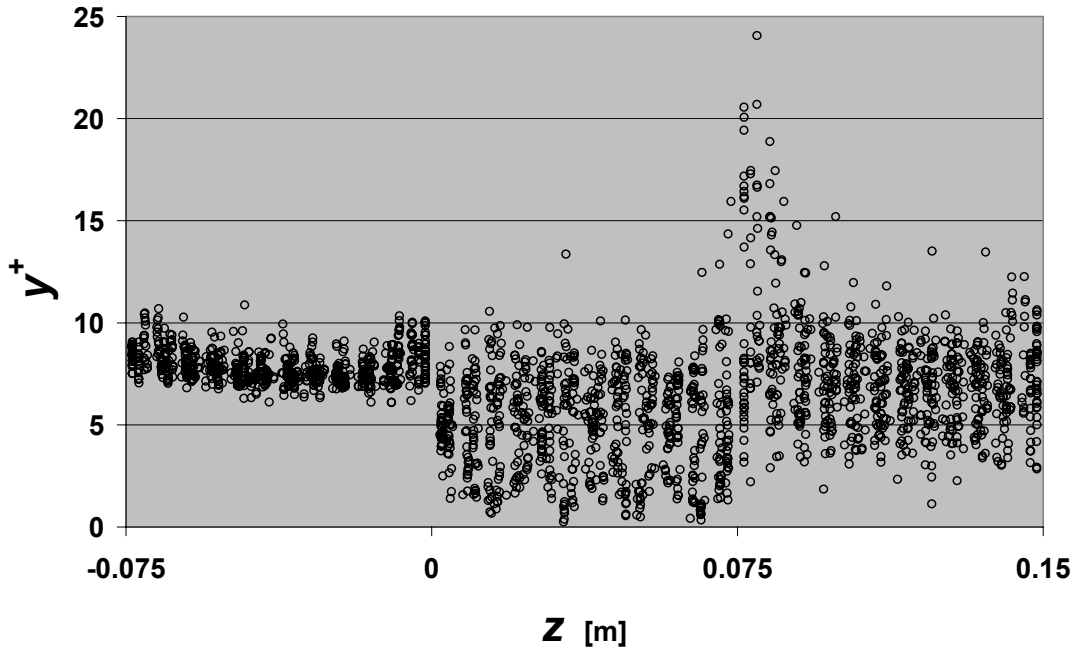


**Figure 4.15.** $y^+$ vs. packed bed height for $Re$ = 912 applying the Spalart – Allmaras turbulence model

Due to the fact that the used version of the Spalart – Allmaras turbulence model incorporates a coupling between wall functions and damping functions, results obtained with this model allowed analyzing $y^+$ values near the cylinder's wall. This model automatically discriminates the use of a wall function or a damping function for modeling *near-wall* flow, which makes it unnecessary to clearly define a priori the mesh density near the wall. It is well known that the

$\kappa-\varepsilon$ models do not work in the *near-wall* region. Normally, for modeling *near-wall* flow with a $\kappa-\varepsilon$ model, it is necessary to use either a wall function or other strategies (e.g. two layer modeling scheme, **TLM**). Choice of one or the other option is governed by the analysis of the $y^+$ parameter. Studies in this area indicate that values of $30 < y^+ < 60$ allow the use of a wall function and values of $1 < y^+ < 5$ allow the use of a **TLM** (Coussirat, 2003). Values of $y^+$ in the cylinder wall for the used mesh for all cases were in the range of $0.2 < y^+ < 25$, making this mesh inadequate for using a wall function or a **TLM** for *near-wall* modeling. An example of the aforementioned can be seen in Figure 4.15.

Figures 4.9 and 4.14 do not show a clear superiority of Spalart – Allmaras turbulence model over the other models tested, but in the case of Figure 4.9, it can be seen that there is a better agreement between Spalart – Allmaras results and Ergun's prediction for pressure drop. A possible explanation for this fact is that factors such as the pressure drop and the radial effective conductivity are not as sensitive to a correct *near-wall* mesh definition as the heat-transfer coefficient, because they are fluid macro-properties that depend on the general velocity profile rather than the *near-wall* velocity profile. In general, velocity profiles for the same velocity inlet conditions and a different turbulence model applied are very similar excepting when you look carefully the *near-wall* velocity field and the boundary layer definition. This fact can be the explanation for the similarity of the values estimated with **CFD** for these parameters, and the slightly better agreement of Spalart–Allmaras model can be justified in the better *near-wall* velocity profile definition achieved when this model is used.

In Figure 4.13, the results obtained with the Spalart – Allmaras model seem to fit better with the empirical correlations than the results obtained with the other two-equation **RANS** models tested. A possible justification for this must be based on the following facts:

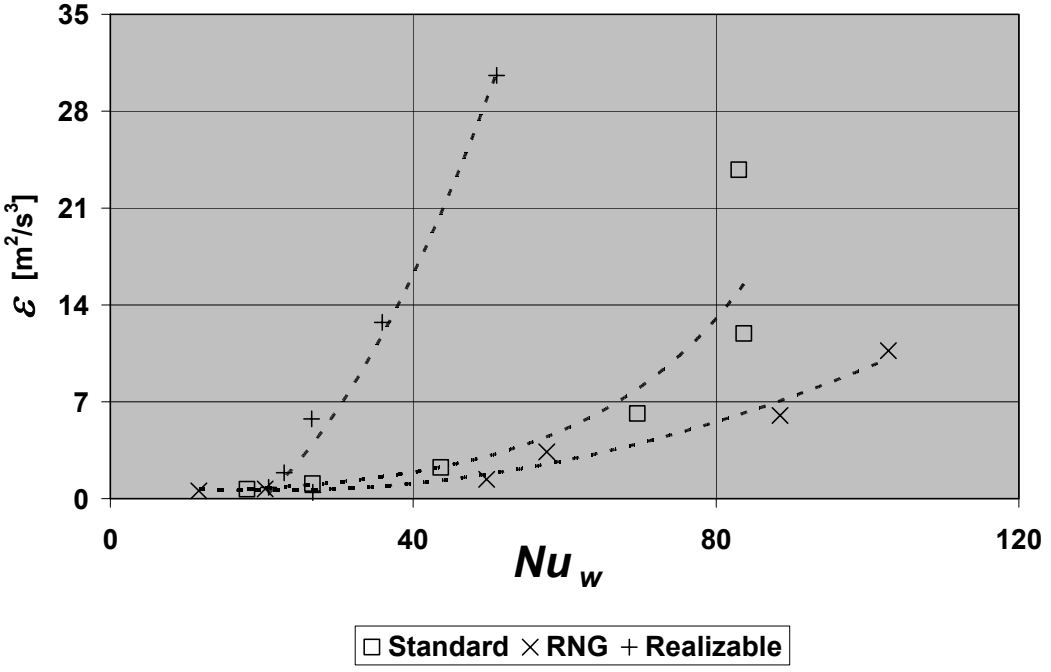


**Figure 4.16.** Turbulent kinetic energy dissipation vs. Nusselt number for $\kappa-\varepsilon$ family models

- The realizable $\kappa-\varepsilon$ model over-estimates the dissipation due to the changes introduced in the turbulent kinetic energy dissipation equation of the model (Figure 4.16). An over-estimated dissipation can be translated as an underestimated mixing in

the flow model and as a consequence of that, heat transfer is also under-estimated in the model.

- Additional diffusion terms in $\kappa - \omega$ model can affect the estimation of heat transfer parameters.

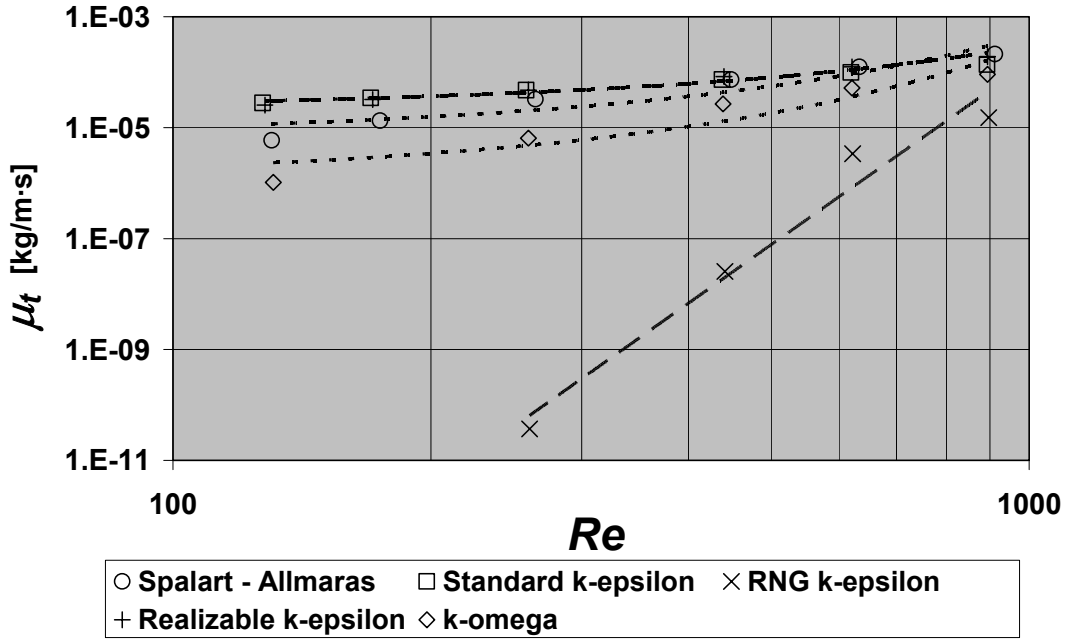


**Figure 4.17.** Turbulent viscosity vs. Reynolds number for different **RANS** models

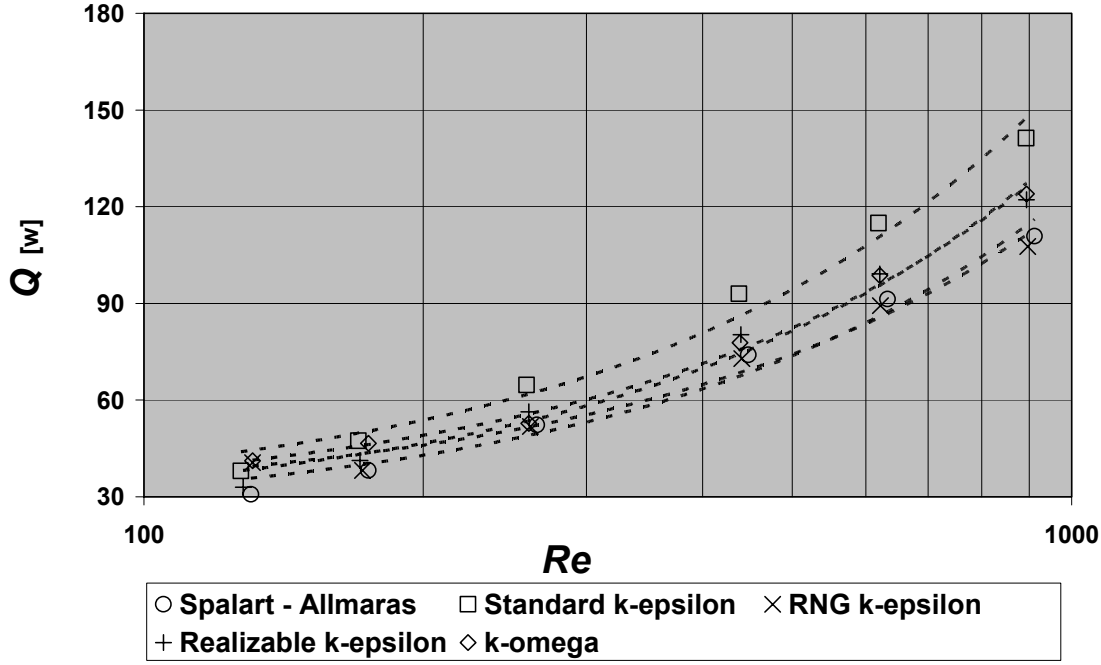


**Figure 4.18.** Heat transfer rate through the wall vs. Reynolds number for different **RANS** models

- **RNG** $\kappa - \varepsilon$ model results reflect the behavior of a rapidly strained flow, which can be noticed in the reduction of $\kappa$ and the under-estimation of the turbulent viscosity (Figure 4.17).

- **CFD** total heat flow estimation is larger for the standard $\kappa - \varepsilon$ model than in the other **RANS** models (Figure 4.18); this must be due to the fact that standard $\kappa - \varepsilon$ model presents a stagnation point anomaly. This means that in a stagnation point, the kinetic energy is over-predicted by the model, enhancing the calculation of the heat flow rate in these areas.

In order to check the grid sensibility of the results, several attempts of varying mesh density near the wall were made, without obtaining an important change in $y^+$ values (see Table 4.4).

| Mesh | $V_{cell}/V_p$ | $y^+$ max | $y^+$ min | $y^+$ average |
|---|---|---|---|---|
| Used mesh | $2.09 \times 10^{-4}$ | 0.2 | 25 | 7.18 |
| Fine mesh 1 | $1.81 \times 10^{-4}$ | 0.1 | 9.7 | 4.38 |
| Fine mesh 2 | $1.53 \times 10^{-4}$ | 0.1 | 10.8 | 4.36 |

**Table 4.4.** $y^+$ analysis for the different meshes tested for the standard $\kappa - \varepsilon$ turbulence model

Figure 4.19 shows the estimation of the heat transfer coefficient with the standard $\kappa - \varepsilon$ turbulence model for three different meshes. It can be noticed that despite the refining of the mesh near the wall, results in the $Nu_w$ estimation do not improve, and as $Re$ increases, there is more divergence between the values obtained for the heat transfer coefficient. This can be due to the fact that refining the mesh near the wall lowers the values for the $y^+$ parameter, and therefore these values get farther from the application range of a wall function for the $\kappa - \varepsilon$ models. Note also that the obtained values for the $y^+$ parameter do not fit into the application range for a **TLM** scheme. A coarser mesh than the one used for simulations (suitable for a correct application of a wall function) could not be obtained due to the presence of highly skewed elements in the small gaps of the geometry. On the other hand, a finer mesh than the ones tested (suitable for a two-layer modeling scheme) could not be obtained because of the high computational demand required for developing and solving it.

Numerically estimated parameters at low $Re$ show discrepancies with those obtained with empirical correlations, and this discrepancy grows as $Re$ becomes lower. In the transition flow regime (approximately $100 < Re < 300$ for fluid flow through a packed bed), results must be observed carefully due to the low capability of **RANS** models to predict the transition from laminar to turbulent flow (Durbin and Petterson Reif, 2001). Rates of convergence became slower as $Re$ decreased and in the models with additional diffusive terms within their formulation.

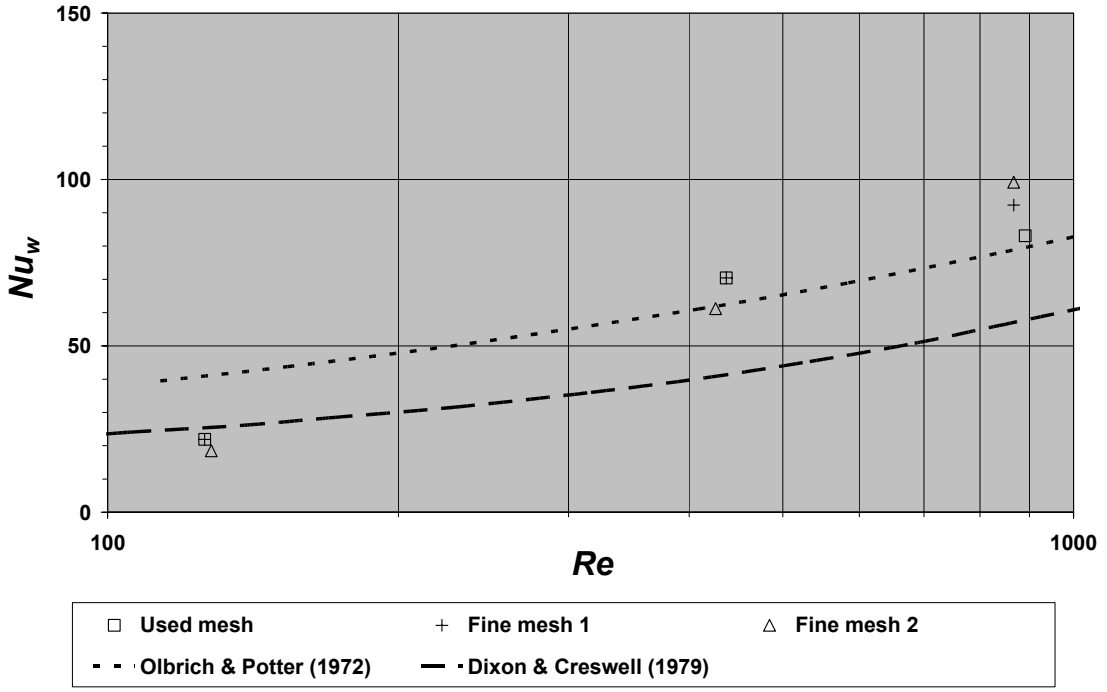


**Figure 4.19.** Heat transfer coefficient estimation for different mesh densities for the standard $\kappa - \varepsilon$ turbulence model

# CONCLUSIONS

**CFD** proves to be useful in the wall to fluid heat transfer parameter estimation, and also for calculation of pressure drop along the bed in packed bed equipment. It was possible to model a realistic case of a packed bed of spheres including contact points within the surfaces involved in the geometry. The calculated velocity profiles fitted qualitatively the expected results, and the calculated values of pressure drop along the bed adjust quite well with previously published and accepted correlations. Flow structures within the bed (i.e., wall channeling, stagnant points, eddy flows) were easily identifiable. Obtained temperature profiles inside the bed allowed estimating wall heat transfer parameters such as $Nu_w$ and $k_t/k_f$ .

The results obtained for all of the cases studied (laminar and turbulent) agree among themselves and with the selected empirical and semi-empirical correlations when analyzing pressure drop and effective radial conductivity. This can be explained by the similarity in the velocity field obtained for each simulation. The calculation of these parameters is more closely related to velocity fields than to mixing parameters. The prediction of the mixing rate within the bed along with the *near-wall* treatment appreciably affects the estimate of Nuw. Flow regime zones can be identified using the heat transfer coefficient estimate. A laminar solution overestimates the value of this coefficient in the turbulent flow zone, and turbulent solutions tend to underestimate the value of the coefficient in the laminar transition zone. Turbulence models used for simulations do not predict the transition regime well, and this can be seen in the discrepancy between numerically obtained results and correlations in the low ***Re*** and transition range.

The definition of a good mesh allows calculations of fluid dynamics variables, as velocity and pressure. However, in our case, the proposed geometry governs mesh density and element size in the *near-wall* area, and this fact affects the definition of an appropriate y+ parameter in order

to apply a correct *near-wall* treatment for certain turbulence models (e.g. the $\kappa - \varepsilon$ family models). To define an adequate $y^+$ for a correct coupling for the two-equation models at the *near-wall* treatment is not an easy task. Therefore, the $y^+$ parameter is crucial during the selection of the appropriate turbulence model to apply within the simulation. A good *near-wall* modeling is fundamental to obtain more accurate results in pressure drop and heat transfer calculations and the selection of the right turbulent model will depend on the geometry proposed and the values obtained for $y^+$ in the wall.

Results obtained with the Spalart–Allmaras turbulence model show better agreement than the two-equation **RANS** models for pressure drop and heat transfer parameter estimation. This could be due to the fact that this model uses a coupling between wall functions and damping functions for *near-wall* treatment, does not include additional diffusion or dissipation terms in its formulation and does not present the stagnation point anomaly. Factors such as the misestimating of $\varepsilon$, $\kappa$ or $\mu_t$ can lead to differences in flow and temperature profiles that can be translated into miscalculation of heat transfer parameters. Therefore, the Spalart – Allmaras model could be a good tool for these kinds of flows because the $y^+$ problem is solved automatically in spite of the necessity of checking the upper values of $y^+$ (less than 120).

Turbulence models used for simulations do not properly predict the transition regime and this can be observed in the discrepancy between numerically obtained results and correlations in the low Re and transition range. Results present slower ratios of convergence at low ***Re*** than at high ***Re***.

# REFERENCES


Coberly, C.A., and Marshall, W.R., (1951). Chemical Engineering Progress, 47, 141.

Coussirat, M., (2003). ***Theoretical/numerical study of flows with strong streamlines curvature***. Ph.D. Thesis. Universitat Politècnica de Catalunya. Barcelona, Spain.

Dalman, M. T., Merkin, J. H., McGreavy, C., (1986). ***Fluid flow and heat transfer past two spheres in a cylindrical tube***. Computers & Fluids, 14, 267 – 281.

Dixon, A.G., and Cresswell, D., (1979). ***Theoretical prediction of effective heat transfer parameters in packed beds.*** AIChE Journal, 25, 663 – 676.

Dixon, A. G., and Nijemeisland, M., (2001). ***CFD as a design tool for fixed-bed reactors.*** Industrial & Engineering Chemistry Research, 40, 5246 – 5254.

Durbin, P.A., and Petterson Reif, B.A., (2001). ***Statistical theory and modeling for turbulent flows.*** John Wiley & Sons, New York. pp. 138 – 139.

Ergun, S., (1952). ***Fluid flow through packed columns.*** Chemical Engineering Progress, 48, 89 – 94.

Fluent Inc., (1998). ***Fluent 5.0 user's guide.*** Fluent Inc.

Graham, R. L., Lubachevsky, B. D., Nurmela, K. J., Östergard, P. R. J., (1998). ***Dense packings of congruent circles in a circle.*** Discrete Mathematics, 181, 139 – 154.

Guardo, A., Larrayoz, M.A., Velo, E., Recasens, F., (2002). ***CFD approach to laminar-to-turbulent flow transition in fixed bed equipment.*** In: Sociedad Española de Química Industrial e

Ingeniería Química/Universitat de Barcelona (Eds). Libro del resúmenes del 9$^0$ Congreso Mediterráneo de Ingeniería Química. Barcelona, Spain. pp. 219.

Guardo, A., Larrayoz, M. A., Recasens, F., (2003). ***Regular packing types for CFD simulation of SCF extraction and reaction equipment***. In: Brunner, G., Kikic, I., Perrut, M., (Eds). Proceedings of the 6$^{th}$ International Symposium on Supercritical Fluids. Institut National Polytechnique: Lorraine, France. pp 643 – 648.

Guedes de Carvalho, J. R. F., and Delgado, J. M. P. Q., (2000). ***Lateral dispersion in liquid flow through packed beds at $Pe_m$ < 1400***. AIChE Journal, 46, 1089 – 1095.

Hatta, S., and Maeda, S., (1948). Kagaku Kogaku, 12, 56.

Jolls, K.R., and Hanratty, T.J., (1966). ***Transition to turbulence for flow through a dumped bed of spheres.*** Chemical Engineering Science, 21, 1185 – 1190.

Kays, W.M., (1994). ***Turbulent Prandtl number. Where are we?*** Journal of Heat Transfer, 116, 284 – 295.

Li, C., and Finlayson, B.A., (1977). ***Heat transfer in packed beds – a reevaluation.*** Chemical Engineering Science, 32, 1055 – 1066.

Lloyd, B., and Boehm, R., (1994). ***Flow and heat transfer around a linear array of spheres.*** Numerical Heat Transfer, Part A, 26, 237 – 252.

Logtenberg, S. A., Nijemeisland, M., Dixon, A. G., (1999). ***Computational fluid dynamics simulations of fluid flow and heat transfer at the wall-particle contact points in a fixed-bed reactor.*** Chemical Engineering Science, 54, 2433 – 2439.

Melissen, H., (1994). ***Densest packing of eleven congruent circles in a circle.*** Geometriae Dedicata, 50, 15 – 25.

Olbrich, W., and Potter, O., (1972). ***Mass transfer from the wall in small diameter packed beds.*** Chemical Engineering Science, 27, 1733 – 1743.

Poling, B., Prausnitz. J., O'Connell, J., (2000). ***The properties of gases and liquids.*** McGraw-Hill, New York. pp. 3.1 – 10.56.

Reid, R., Prausnitz, J., Poling, B., (1987). ***The properties of gases and liquids.*** McGraw-Hill, Boston. pp. 95 – 205.

Suekane, T., Yokouchi, Y., Hirai, S., (2003). ***Inertial flow structures in simple-packed bed of spheres.*** AIChE Journal, 49, 10 – 17.

Tobis, J., and Ziólkowski, D., (1988). ***Modelling of heat transfer at the wall of a packed-bed apparatus.*** Chemical Engineering Science, 43, 3031 – 3036.

White, F., (1991). ***Viscous fluid flow.*** McGraw-Hill, New York. pp. 482 – 542.

Yaws, C., (1999). ***Chemical properties handbook.*** McGraw-Hill, New York. pp. 1 – 55.